

Himalayan tectonics explained by extrusion of a low-viscosity crustal channel coupled to focused surface denudation

C. Beaumont*, R.A. Jamiesont, M.H. Nguyen*†, and B. Lee*

*Department of Oceanography, Dalhousie University, Halifax, N.S., Canada, B3H 4J1

†Department of Earth Sciences, Dalhousie University, Halifax, N.S., Canada, B3H 3J5

Recent interpretations of Himalayan-Tibetan tectonics have proposed that channel flow in the middle to lower crust can explain outward growth of the Tibetan plateau^{1,2,3}, and that ductile extrusion of high-grade metamorphic rocks between coeval normal- and thrust-sense shear zones can explain exhumation of the Greater Himalayan sequence^{4,5,6,7}. Here we use coupled thermal-mechanical numerical models to show that these two processes - channel flow and ductile extrusion - may be dynamically linked through the effects of surface denudation focused at the edge of a plateau that is underlain by low-viscosity material. Our models provide an internally self-consistent explanation for many observed features of the Himalayan-Tibetan system^{8,9,10}.

Figure 1 shows a general cross-section highlighting features of the orogen (numbers 1-9) requiring explanation in any quantitative model¹⁰. These include contemporaneous north-south shortening on the Main Central Thrust (MCT) system (1) and extension along the South Tibetan Detachment (STD) system (2), the creation of gneiss domes (3) in the southern Tibetan plateau, the style

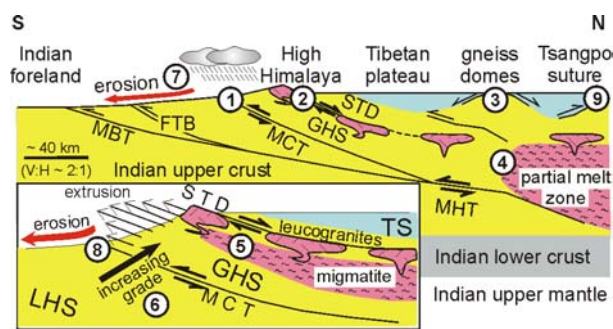


Figure 1. General tectonic features of the Himalaya and southern Tibet^{5,8-10,15,16}. Numbers 1-9 correspond to important features requiring explanation¹⁰; see Fig. 2-4 for corresponding features of models. Inset shows southern flank of Tibetan plateau (not to scale) with geological features discussed in text. LHS, Lesser Himalayan sequence; GHS, Greater Himalayan sequence; TS, Tethyan sequence; MCT, Main Central Thrust; STD, South Tibetan Detachment; MHT, Main Himalayan Thrust; MBT, Main Boundary Thrust; FTB, fold-thrust belt (Siwaliks). Colours (all figures): blue, weak upper crust; yellow, medium-strength middle crust; grey, strong lower crust; pink, melt-weakened middle crust (includes migmatite and plutons).

and timing of metamorphism in the Greater Himalayan (GHS, 5) and Lesser Himalayan (LHS, 6) sequences, and the juxtaposition of contrasting protoliths (8) across the MCT zone. We show below that these disparate observations can all be interpreted to result from coupling between channel flow originating in partially molten crust beneath Tibet (4) and rapid denudation of the south flank of the Himalaya (7).

We first present the behaviour of a reference model (Model 1; Fig. 2), and demonstrate a similar tectonic style with boundary conditions appropriate for the Himalayan-Tibetan system (Model 2; Fig. 2). The sensitivity of the model results to surface denudation rate and upper crustal rheology is investigated (Fig. 3), and results compatible with observations from a generalised Himalayan cross-section are presented (Model 3, Fig. 4). The models build on our earlier mechanical¹¹ and thermal-mechanical^{12,13} results. In the context of the Himalayan-Tibetan system (Fig. 1), 'pro'-lithosphere, corresponding to India, converges on stationary 'retro'-lithosphere, corresponding to Asia, at velocity V_p . Pro-mantle lithosphere is detached and subducted at point S (Fig. 2; details in caption and Supplementary Information); the model 'suture' is the initial boundary between pro- and retro-crust. Surface denudation rate depends on local surface slope, time, and a spatial climate function^{12,13} (Fig. 2; details in caption) that yields high denudation rates on the steep pro-ward flank of the plateau, corresponding to the Himalaya, and low to negligible rates elsewhere. The most important model property is an extra increment of weakening in the upper crust^{12,13} such that effective viscosity is reduced linearly from the power law flow value¹⁴ at 700°C to 10^{19} Pa.s at $T \geq 750^\circ\text{C}$, a factor of about 10. This is probably a conservative estimate for weakening by a small amount of *in situ* partial melt, here referred to as 'melt weakening'.

Figure 2 illustrates interactions among temperature, rheology, channel flow, and surface denudation. Model 1 (basic subduction) has $V_p = 2$ cm/y, whereas Model 2 (advancing subduction) has $V_p = 5$ cm/y, $V_s = 2.5$ cm/y (Fig. 2), and includes subduction of lower pro-crust. Initial conditions and early evolution are described elsewhere¹³ (see Supplementary Information). Note that despite the different boundary conditions, both models have similar channel-denudation interactions at the denudation front (Fig. 2f,j). For large convergence ($\Delta x > 1000$ km) the 70-75 km thick crust has a well developed plateau and much of the middle to lower crust is above 700°C. Reverse channel flow (Fig. 2c,i) develops where hot upper crust is melt weakened and is subject to a pressure gradient developed between the plateau and the foreland^{1,2,3,12,13}.

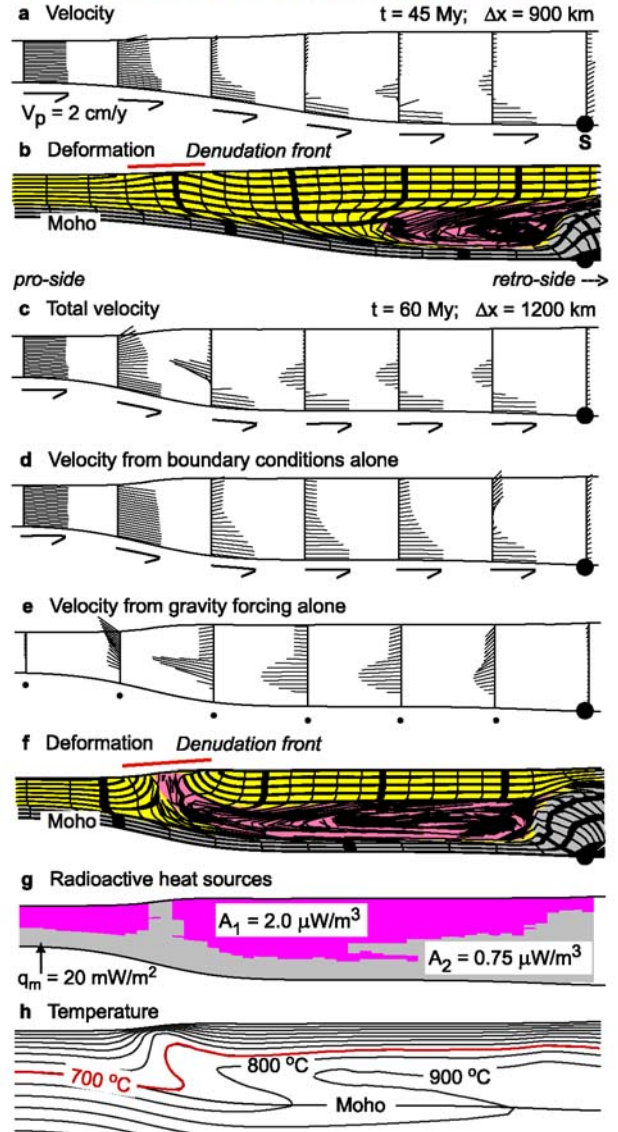
Initially, the channel flow propagates ('tunnels') through the converging pro-crust (Fig. 2a,b) at a rate controlled by the temperature increase and associated viscosity decrease at the channel tip^{12,13}. By $\Delta x = 1200$ km, efficient erosion of the pro-flank of the plateau leads to coupling between channel flow and surface denudation (Fig. 2f). Channel velocity increases and the channel is exhumed at the erosion front in a narrow zone bounded by upper normal-

sense and lower thrust-sense shear zones (Fig. 2f). Isotherms are advected pro-ward by channel flow and condensed near the surface by cooling accompanying denudation (Fig. 2g,h). Decomposing the total velocity

field (Fig. 2c) into tectonic and gravitational components¹² (Fig. 2d,e) shows that gravity forces drive the channel flow.

Figure 2. Development of surface-coupled channel flow (a-h) and effect of changing convergence velocity and subduction conditions (i-j). Pro-side is to left in all panels; retro-side lies to right of S and is generally not shown; see also Supplementary Information. Colours as for Fig. 1 unless otherwise noted. Model 1 ($V_P = 2$ cm/y; $V_S = 0$; no crust subducted): **a**) crustal velocity field at 45 My, showing reverse flow in mid-crust, basal velocity (arrows) and detachment point (S); **b**) deformed passive marker grid (45 My), showing 'tunneling' of channel before coupling to surface denudation; **c**) crustal velocity field at 60 My, showing reverse channel flow coupled to surface denudation; **d**) retro-ward velocity resulting from basal boundary conditions alone; **e**) pro-ward velocity resulting from gravitational forcing; **f**) deformed marker grid (60 My) showing extrusion of channel at denudation front; **g**) corresponding distribution of radioactive material in crust (magenta, A_1 , high heat production; grey, A_2 , lower heat production); **h**) crustal isotherms, showing lateral advection of hot material in channel; 700°C isotherm (red) marks onset of melt weakening. Model 2 shows effect of lower crustal subduction and partitioning of basal velocity, $V_P = 5$ cm/y, into subduction and subduction zone advance (V_S at 2.5 cm/y each (V_S is the rate the subduction point S moves in the retro-direction)): **i**) crustal velocity field at 51 My; **j**) deformed marker grid at same time, showing channel extrusion as in f and position of suture (9). Heat balance equation: $\rho C_p(\partial T/\partial t + \underline{v} \cdot \nabla T) = K \nabla^2 T + A$; thermal parameters (same for all models, see also **g**): asthenospheric $T_a = 1,350^\circ\text{C}$; specific heat at constant pressure $C_p = 750$ m²/°Ks²; $\rho_{\text{crust}} = 2700$ kg/m³; $\rho_{\text{mantle}} = 3300$ kg/m³; thermal conductivity $K = 2.0$ W/m°K; thermal diffusivity $\kappa = 1.0 \times 10^{-6}$ m²/s. A is the volumetric radioactive heat production. Flexural rigidity = 10^{22} Nm. Ductile flow law: $\eta = B^* (\dot{\epsilon})^{1/n - 1} \exp(Q^*/nRT)$, where η is effective viscosity, B^* is the pre-exponential coefficient, n is the power-law coefficient, $\dot{\epsilon}$ is the second invariant deviatoric strain rate, and Q^* is the activation energy. Coulomb (frictional) flow law: effective internal angle of friction, $\phi = 15^\circ$. Upper crustal rheology (0-25 km): 'wet' Black Hills quartzite¹⁴, $n = 4.0$, $Q^* = 223$ kJ/mol, $B^* = 2.92 \times 10^6$ Pa.s^{1/4}; 'melt weakening': effective viscosity decreases from flow law value at 700°C to $\eta = 10^{19}$ Pa.s at $T \geq 750^\circ\text{C}$; lower crustal rheology (25-35 km): 'dry' Maryland diabase³⁰ with $B^*/10$, $n = 4.7$, $Q^* = 485$ kJ/mol, $B^* = 1.91 \times 10^5$ Pa.s^{1/4.7}. Denudation rate: 0 for $t < 37.5$ My; for $t > 37.5$ My = $0.107 \times \text{slope} \times g(x)$ m/y, where $g(x) = 0$ at $x > 500$ km, $g(x) = 1$ at $x < 450$ km, linear decrease in $g(x)$ from 1 to 0 between 450-500 km. This represents humid to arid transition between foreland and plateau, and gives denudation rates of about 1 cm/y for slopes of 1:10 (averaged on 10 km horizontal scale).

Model 1: Development of Crustal Channel/Extrusion



The two models have similar thermal-tectonic styles in the region that corresponds to the Himalaya and southern Tibetan plateau, demonstrating relative insensitivity to the choice of boundary conditions. Model 2 ($V_p = 5$ cm/y, $V_s = 2.5$ cm/y) is more compatible with the average 5 cm/y post-collision convergence rate of India relative to Asia^{10,15}, and at 51 My also has properties consistent with observed crustal thickness, plateau width, suture position^{15,16} (Fig. 2i,j), extent of underthrust pro-mantle (Indian) lithosphere as inferred seismically¹⁶, and temperature distribution (similar to Fig. 2h). However, the broadly symmetrical geometry of both models at the denudation front (Fig. 2f,j) contrasts with typical asymmetrical Himalayan structures. Factors affecting the range of model styles, including symmetry, are addressed below.

The model results are sensitive to variations in surface denudation rate and upper crustal rheology, leading to a variety of predicted flow modes (Fig. 3; details in caption). Changes in denudation rate affect the degree of coupling between the surface and the channel, and the presence of a weak upper crustal layer, analogous to a sedimentary sequence overlying crystalline crust, affects the mechanical behaviour of the crust above the channel. Although melt weakening to 10^{19} Pa.s is required to initiate and sustain channel flow, further viscosity reduction to 10^{18} Pa.s does not strongly influence the model results¹². Some of the predicted flow modes may be comparable to different regions or evolutionary stages of the Himalayan-Tibetan system.

In the absence of denudation the channel flow tunnels through converging crust^{12, 13} (Fig. 3a), as has been proposed to explain eastward propagation of the Tibetan plateau^{1,2,3}. Denudation focused on the plateau flank leads to symmetrical exhumation when the upper crust does not detach above the channel (Models 1, 2; Fig. 3b), possibly analogous to the Nanga Parbat region¹⁷. Detachment of weak upper crust and its outward flow with the channel creates asymmetric thrust extrusion, as observed in the Himalaya^{7,10} (Fig. 3c). Underthrusting of cold crust beneath the exhumation front and into the channel (Fig. 3d) creates a master thrust zone between underthrust lower crust and

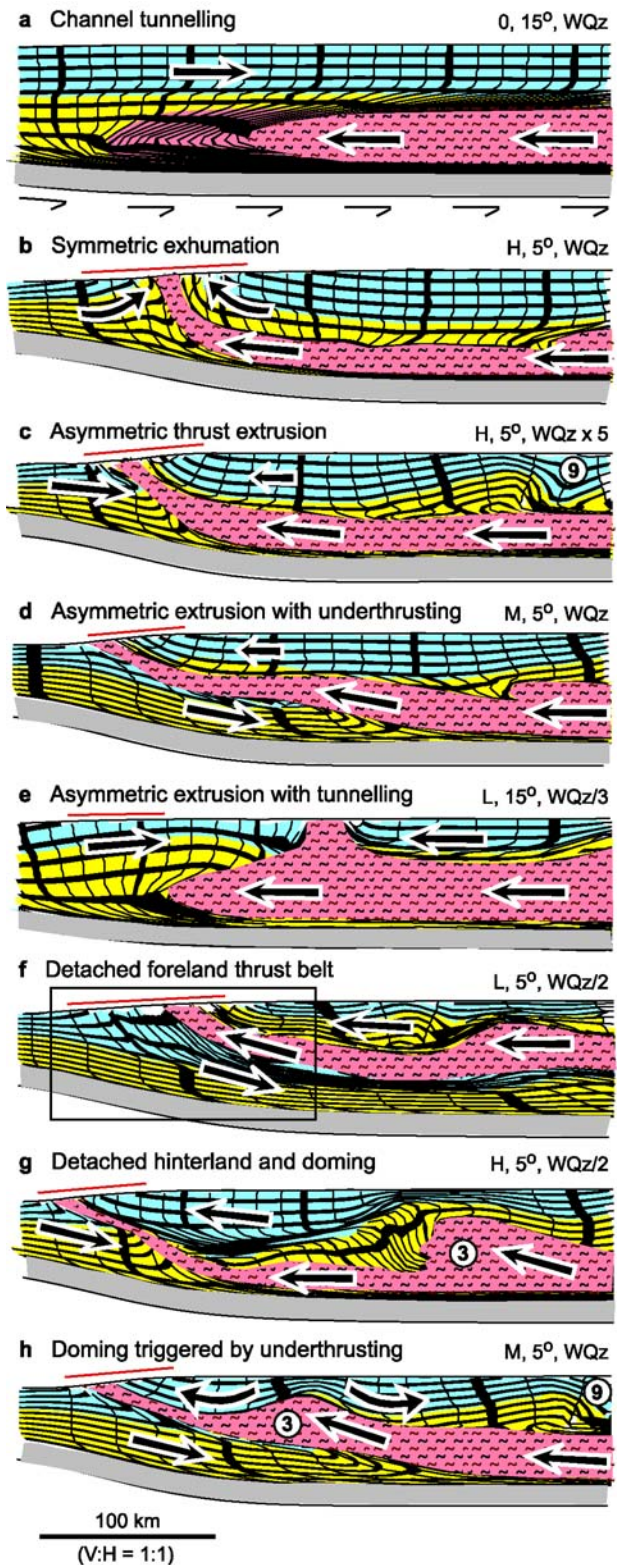


Figure 3. Model channel flow modes and exhumation/extrusion styles. Properties as for Model 2 except for upper crustal rheology (blue; $\phi = 5^\circ$ or 15° ; WQz, wet quartzite flow law¹⁴, effective viscosity scaled as shown) and erosion rate, which ranges from 0 to low (L, <0.4 cm/y), moderate (M, 0.4 - 1.4 cm/y), or high (H, >1.4 cm/y) where surface slope is maximum for the time step shown. **a**) Channel tunnelling, no denudation^{12,13}; **b**) symmetric exhumation (Models 1, 2); **c**) asymmetric thrust extrusion; **d**) asymmetric extrusion with underthrusting; **e**) asymmetric extrusion with tunnelling; abandoned extrusion zone translated into plateau; **f**) detached foreland fold-thrust belt; box outlines region similar to that shown in Fig. 4; **g**) detached hinterland followed by doming and extension; **h**) dome triggered by underthrusting. Colours as for Fig. 1; red line above model surface indicates denudation front; pink indicates melt-weakened channel flow zone (strongly deformed grid removed for clarity); arrows show flow direction; (3) indicates structures resembling north Himalayan gneiss domes¹⁹; (9) indicates suture.

the channel, analogous to the inferred Main Himalayan Thrust^{9,15,16} (MHT, Fig. 1, 4c). A significant reduction in denudation rate can lead to abandonment of the extrusion zone and re-establishment of channel tunnelling (Fig. 3e). For sufficiently weak upper crust and low erosion rates the foreland detaches to form a fold-thrust belt, analogous to

the Siwaliks¹⁸, in front of the exhuming channel (Fig. 3f). Detachment of weak upper crust on the hinterland side of the erosion front leads to doming of the channel beneath the extending and thinning upper crust (Fig. 3g); doming may also be triggered when underthrust crust (Fig. 3d) uplifts and squeezes the channel, causing extension in destabilised upper crust (Fig. 3h). Domes created in this way lie between the suture (9) and the denudation front, and may be equivalent to gneiss domes (3), including the Kangmar dome¹⁹, associated with the north Himalayan antiform¹⁰.

Figure 4 compares the results of a model with weak upper crust and variable denudation rate (Model 3) to observations from the Himalaya of central Nepal (corresponding numbers, Fig. 1, 4). Early stages of Model 3 (not shown) are similar to Models 1 and 2. Channel flow is initiated by the development of low viscosity material in the hot crust beneath the plateau (4), as has been inferred for Tibet⁹. Coeval thrust- and normal-sense distributed shear across the lower and upper parts of the channel (Fig. 4c) are interpreted to correspond to top-to-the-south motion on the MCT (1) and top-to-the-north motion along the STD (2), respectively. Coupling between focused surface denudation and channel flow leads to ductile extrusion of hot channel material, represented in nature by the high-grade migmatitic gneisses of the GHS (5) lying between the MCT and STD^{4,5,6,7}. Focused surface denudation (7) of the GHS on the steep windward flank of the Tibetan plateau is required to exhume the channel, consistent with isotopic and detrital mineral data indicating that the GHS or equivalent rocks have been actively eroded since the early Miocene^{18,20,21}.

Processes associated with channel extrusion can explain many features of the MCT zone, including the 'inverted' metamorphic profile¹⁰ (6), contrasting metamorphic ages across the MCT^{10,22}, and contrasts in age and provenance of GHS and LHS protoliths^{23,24} (8). Model peak grade profiles (Fig. 4a,b) agree well with pressure-temperature (P-T) data from the MCT zone and GHS in central Nepal^{25,26,27}. In Model 3, denudation rate progressively decreases during the last 15 My, as inferred for the Himalaya^{20,28}; this produces an age pattern (Fig. 4b) that is compatible with young ages (<10 Ma) reported from the LHS²² and generally older ages (>15 Ma) from the GHS^{28,29}. The peak grade profiles and age distributions result from the juxtaposition of contrasting rock packages (8a,b,c, Fig. 4c) across the lower boundary of the channel and from distributed ductile shear within the channel and its footwall. Selected particle trajectories and P-T-t paths (Fig. 4d,e) illustrate how points originating in different parts of the system, and following different trajectories through the evolving thermal structure of the orogen, can be exhumed together at the orogenic front. These points correspond to (A) LHS rocks buried in the channel footwall and exhumed adjacent to the channel, (B) lower GHS rocks transported into the orogen and later extruded by reverse channel flow, and (C) upper GHS rocks buried near the onset of orogenesis and extruded in the upper part of the channel. In the model, crustal segments initially separated by more than 600 km (8a, 8b; Fig. 4c) have been juxtaposed across the MCT. By implication, the MCT is

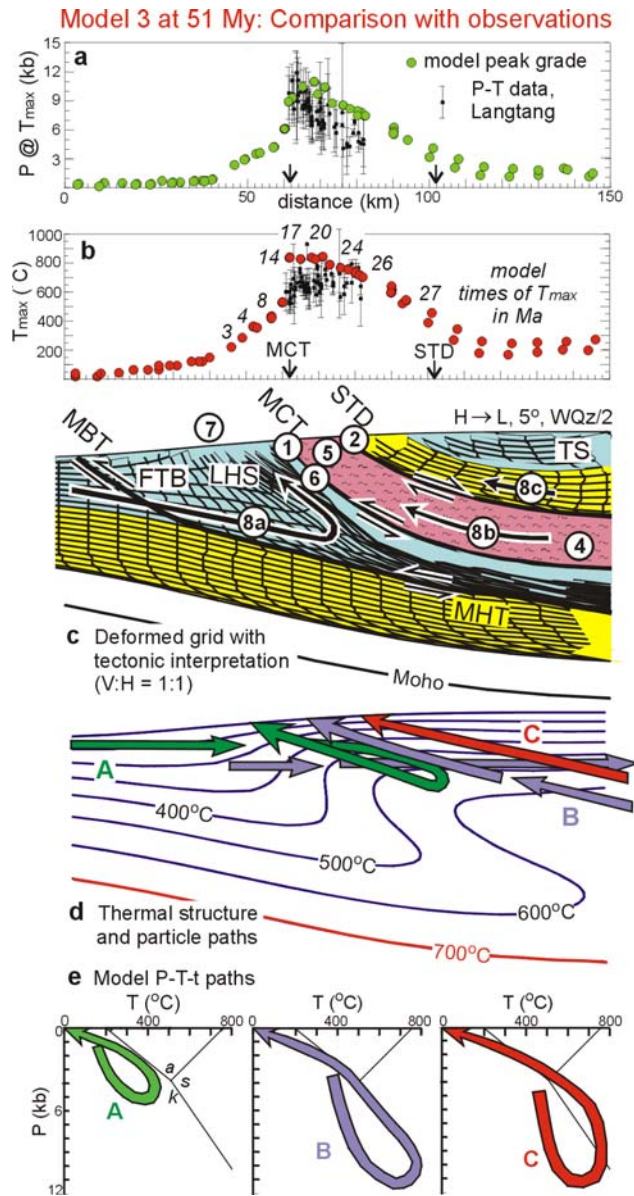


Figure 4. Comparison of Model 3 (51 My) with observations from the Himalayan-Tibetan system. Large-scale features (for example, positions of suture and S-point) are similar to Model 2 (Fig. 2j). **a)** Pressure P at T_{\max} profile (green) compared with P data from the Langtang region, central Nepal^{25,26,27}, where T_{\max} is the maximum temperature reached by the points shown during the evolution of the model; arrows show observed positions of the MCT and STD; **b)** T_{\max} profile (red) compared with T data from the same area; numbers are model times of T_{\max} in Ma; **c)** deformed marker grid and tectonic interpretation (see text); numbers, colours, and abbreviations as in Fig. 1; rheology and erosion rates as in Fig. 3; 8a, 8b, 8c represent contrasting rock units following trajectories shown by black arrows; **d)** isotherms at 51 My and particle paths (green, purple, red arrows) for points originating in different parts of the model that are exhumed together at ca. 51 My; note that orogen and isotherms advance toward foreland with time; **e)** model P-T-t paths for points shown in **d)**; reference lines show stability fields of andalusite (a), kyanite (k), and sillimanite (s). Panels **a-d** aligned at MCT; horizontal distance between MCT and STD is sensitive to local structure and topography, but model channel thickness (10-15 km) is similar to inferred structural thickness of GHS^{7,28}.

both a structural and protolith boundary^{4,7,23,24}.

These models, to our knowledge, represent the first quantitative demonstration that flow in a low-viscosity crustal channel that is coupled to surface denudation provides an internally consistent explanation not only for ductile extrusion of the GHS but for many other salient features of the Himalayan-Tibetan system. The critical factors are the presence of low viscosity material in the middle to lower crust, a variation in crustal thickness between plateau and foreland, and surface denudation that is focused on the plateau flank. The range of model styles, and by implication the tectonics of natural orogens, is sensitive to variations in denudation rate and upper crustal strength.

References

1. Royden, L.H. Coupling and decoupling of crust and mantle in convergent orogens: implications for strain partitioning in the crust. *J. Geophys. Res.* **101**, 17679-17705 (1996).
2. Clark, M.K. & Royden, L.H. Topographic ooze: Building the eastern margin of Tibet by lower crustal flow. *Geology* **28**, 703-706 (2000).
3. Shen, F., Royden, L.H. & Burchfiel, B.C. Large-scale crustal deformation of the Tibetan Plateau. *J. Geophys. Res.* **106**, 6793-6816 (2001).
4. Grujic, D. *et al.* Ductile extrusion of the Higher Himalayan Crystalline in Bhutan: evidence from quartz microfabrics. *Tectonophysics* **260**, 21-43 (1996).
5. Wu, C. *et al.* Yadong cross structure and the South Tibetan Detachment in the east central Himalaya (89°-90°E). *Tectonics* **17**, 28-45 (1998).
6. Vannay, J-C. & Grasemann, B. Himalayan inverted metamorphism and syn-convergence extension as a consequence of a general shear extrusion. *Geol. Mag.* **138**, 253-276 (2001).
7. Grujic, D., Hollister, L.S. & Parrish, R.R. Himalayan metamorphic sequence as an orogenic channel: Insight from Bhutan. *Earth Planet. Sci. Lett.* (in press).
8. Burchfiel, B.C. *et al.* The South Tibetan detachment system, Himalayan orogen: Extension contemporaneous with and parallel to shortening in a collisional mountain belt. *Geol. Soc. Am. Spec. Pap.* **269**, 41 pp. (1992).
9. Nelson, K.D. *et al.* Partially molten middle crust beneath southern Tibet: a synthesis of Project INDEPTH results. *Science* **274**, 1684-1688 (1996).
10. Hodges, K.V. Tectonics of the Himalaya and southern Tibet from two perspectives. *Geol. Soc. Am. Bull.* **112**, 324-350 (2000).
11. Willett, S.D., Beaumont, C. & Fullsack, P. Mechanical model for the tectonics of doubly vergent compressional orogens. *Geology* **21**, 371-374 (1993).
12. Beaumont, C., Jamieson, R.A., Nguyen, M.H. & Lee, B. Mid-crustal channel flow in large hot orogens: results from coupled thermal-mechanical models. in *Slave - Northern Cordillera Lithospheric Evolution (SNORCLE) and Cordilleran Tectonics Workshop* (compiled by Cook, F. & Erdmer, P.) 112-170 (Lithoprobe Report **79**, 2001).
13. Jamieson, R.A., Beaumont, C., Nguyen, M.H. & Lee, B. Interaction of metamorphism, deformation, and exhumation in large convergent orogens. *J. Met. Geol.* **20**, 1-16 (2002).
14. Gleason, G.C. & Tullis, J. A flow law for dislocation creep of quartz aggregates determined with the molten salt cell. *Tectonophysics* **247**, 1-23 (1995).
15. Hauck, M.L., Nelson, K.D., Brown, L.D., Zhao, W. & Ross, A.R. Crustal structure of the Himalayan orogen at ~90° east longitude from Project INDEPTH deep reflection profiles. *Tectonics* **17**, 481-500 (1998).
16. Owens, T.J. & Zandt, G. Implications of crustal property variations for models of Tibetan plateau evolution. *Nature* **387**, 37-43 (1997).
17. Zeitler, P.K. *et al.* Crustal reworking at Nanga Parbat, Pakistan: Metamorphic consequences of thermal-mechanical coupling facilitated by erosion. *Tectonics* **20**, 712-718 (2001).
18. DeCelles, P.G. *et al.* Stratigraphy, structure, and tectonic evolution of the Himalayan fold-thrust belt in western Nepal. *Tectonics* **20**, 487-509 (2001).
19. Lee, J. *et al.* Evolution of the Kangmar Dome, southern Tibet: Structural, petrologic, and thermochronologic constraints. *Tectonics* **19**, 872-895 (2000).
20. White, N.M. *et al.* Constraints on the structural evolution, exhumation, and erosion of the High Himalayan Slab, NW India, from foreland basin deposits. *Earth Planet. Sci. Lett.* (in press).
21. France-Lanord, C., Derry, L. & Michard, A. Evolution of the Himalaya since Miocene time: Isotopic and sedimentological evidence from the Bengal Fan. in *Himalayan Tectonics* (eds. Treloar, P.J. & Searle, M.P.) 603-621 (Geological Society Special Publication **74**, 1993).
22. Harrison, T.M. *et al.* A Late Miocene-Pliocene origin for the central Himalayan inverted metamorphism. *Earth Planet. Sci. Lett.* **146**, E1-E7 (1997).
23. Parrish, R.R. & Hodges, K.V. Isotopic constraints on the age and provenance of the Lesser and Greater Himalayan sequences, Nepalese Himalaya. *Geol. Soc. Am. Bull.* **108**, 904-911 (1996).
24. DeCelles, P.G., Gehrels, G.E., Quade, J., LaReau, B. & Spurlin, M. Tectonic implications of U-Pb zircon ages of the Himalayan orogenic belt in Nepal. *Science* **288**, 497-499 (2000).
25. Inger, S. & Harris, N.B.W. Tectonothermal evolution of the High Himalayan Crystalline Sequence, Langtang Valley, northern Nepal. *J. Met. Geol.* **10**, 439-452 (1992).
26. Macfarlane, A.M. An evaluation of the inverted metamorphic gradient at Langtang National Park, central Nepal Himalaya. *J. Met. Geol.* **13**, 595-612 (1995).
27. Fraser, G., Worley, B. & Sandiford, M. High-precision geothermobarometry across the High Himalayan

metamorphic sequence, Langtang Valley, Nepal. *J. Met. Geol.* **18**, 665-682 (2000).

28. Searle, M.P. *et al.* Shisha Pangma leucogranite, South Tibetan Himalaya: Field relations, geochemistry, age, origin, and emplacement. *J. Geol.* **105**, 307-326 (1997).

29. Hodges, K.V., Parrish, R.R. & Searle, M.P. Tectonic evolution of the central Annapurna range, Nepalese Himalaya. *Tectonics* **15**, 1264-1291 (1996).

30. Mackwell, S.J., Zimmerman, M.E. & Kohlstedt, D.L. High-temperature deformation of dry diabase with application to tectonics on Venus. *J. Geophys. Res.* **103**, 975-984 (1998).

Supplementary Information accompanies the paper on Dalhousie Geodynamics Group website (<http://adder.ocean.dal.ca>) and on Nature's website (<http://www.nature.com>).

Acknowledgements

This research was funded by Lithoprobe Supporting Geoscience and NSERC Research grants to C.B. and R.A.J., and the Inco Fellowship of the Canadian Institute for Advanced Research to C.B.. All the models are run using the finite element thermal-mechanical program developed by P. Fullsack. The work has benefited from helpful discussions with J. Braun, L. Brown, L. Derry, P. Fullsack, D. Grujic, D. Nelson, S. Medvedev, O. Vanderhaeghe, and K. Whipple. Constructive reviews by L. Royden and an anonymous referee substantially improved the manuscript.

Correspondence and requests for materials should be addressed to C. Beaumont (Chris.Beaumont@Dal.Ca)